# Low-order modeling of wind farm aerodynamics using leaky Rankine bodies

Daniel B. Araya, Anna E. Craig, Matthias Kinzel, and John O. Dabiri

**Articles you may be interested in**

# Low-order modeling of wind farm aerodynamics using leaky Rankine bodies

Daniel B. Araya,[1] Anna E. Craig,[2] Matthias Kinzel,[1] and John O. Dabiri[1,3,a]

[1]*Graduate Aerospace Laboratories, California Institute of Technology, Pasadena, California 91125, USA*
[2]*Applied Physics, California Institute of Technology, Pasadena, California 91125, USA*
[3]*Bioengineering, California Institute of Technology, Pasadena, California 91125, USA*

We develop and characterize a low-order model of the mean flow through an array of vertical-axis wind turbines (VAWTs), consisting of a uniform flow and pairs of potential sources and sinks to represent each VAWT. The source and sink in each pair are of unequal strength, thereby forming a "leaky Rankine body" (LRB). In contrast to a classical Rankine body, which forms closed streamlines around a bluff body in potential flow, the LRB streamlines have a qualitatively similar appearance to a separated bluff body wake; hence, the LRB concept is used presently to model the VAWT wake. The relative strengths of the source and sink are determined from first principles analysis of an actuator disk model of the VAWTs. The LRB model is compared with field measurements of various VAWT array configurations measured over a 3-yr campaign. It is found that the LRB model correctly predicts the ranking of array performances to within statistical certainty. Furthermore, by using the LRB model to predict the flow around two-turbine and three-turbine arrays, we show that there are two competing fluid dynamic mechanisms that contribute to the overall array performance: turbine blockage, which locally accelerates the flow; and turbine wake formation, which locally decelerates the flow as energy is extracted. A key advantage of the LRB model is that optimal turbine array configurations can be found with significantly less computational expense than higher fidelity numerical simulations of the flow and much more rapidly than in experiments. © *2014 AIP Publishing LLC*. [http://dx.doi.org/10.1063/1.4905127]

## I. INTRODUCTION

There is a persistent need for simple yet reliable models of wind turbine aerodynamics that can aid in the design of wind farms. Originating with the work of Rankine,[1] actuator disk theory is perhaps the most widely used example of such a model.[2–4] It represents an individual turbine rotor as an infinitely thin permeable disk whose extent is defined by the rotor swept area. The energy extraction process is idealized to take place at the disk, resulting in induced streamwise velocity variations ahead of and behind the turbine. Betz[5] used this concept along with one-dimensional linear momentum theory and Bernoulli's principle to derive the well-known theoretical limit to the amount of energy that can be extracted from the flow upstream of a horizontal-axis wind turbine (HAWT), which is approximately 59%. Lissaman[6] also used linear momentum theory and a semi-empirical wake model to investigate the performance of large arrays of HAWTs by superposing multiple model wakes together. A numerical sensitivity analysis showed the effects of streamwise and crosswind HAWT spacing as well as ambient turbulence, turbine hub height ratio, and other turbine characteristics on array performance.[7] This work demonstrated that streamwise spacing and ambient turbulence are primary factors that determine array efficiency. Modern wind farms are typically comprised of HAWTs that are

---

a)Electronic mail: jodabiri@caltech.edu

     **6**, 063118-1     

spaced approximately 3–5 rotor diameters (D) in the cross-wind direction and 6–10 D in the streamwise direction. This spacing is an effort to mitigate performance losses due to turbine wake interactions.[8] A more recent optimization study of HAWT spacing using Large Eddy Simulation (LES) suggests an even larger optimal streamwise spacing of approximately 15 D.[9]

While large HAWT spacing may optimize the power production of each turbine in the array, it potentially reduces the amount of power that can be extracted from a given wind farm footprint. The footprint power density can be an important design constraint in areas where land is limited, such as near population centers, or where the source of wind is isolated to a narrow region of terrain, such as along a ridgeline or shoreline. Vertical-axis wind turbines (VAWTs), whose rotor blades spin on an axis perpendicular to the ground, have recently been suggested to achieve higher turbine power output per unit land area than HAWTs.[10,11] This is in part due to the fact that, unlike for HAWTs, it is possible to increase the swept area of a VAWT independent of its footprint. Despite the more complex aerodynamics of VAWTs as compared to HAWTs, there have been significant efforts made to improve the modeling of VAWT aerodynamics. The methods, mostly developed in the 1970 s, can be classified into three categories: (1) momentum methods, including variants of single and multiple streamtube models; (2) vortex methods, where the effect of the turbine on the flow is modeled using sheets of discrete vorticity; and (3) local-circulation methods, which include some of the features of the other two methods. Detailed summaries of each of the methods are given by Touryan *et al.*[12] and also in a more recent review by Islam *et al.*[13] Of particular note is the work of Templin,[14] who introduced a single streamtube model for VAWTs, following the same actuator disk theory used by Betz. Specifically, the streamwise forces on the VAWT rotor blades are equated to the change in streamwise wind momentum. This results in an induced velocity that is assumed to be constant through the rotor, which is itself replaced by an equivalent actuator disk. Computational work by Martinelli and Smits[15] as well as Shamsoddin and Porté-Agel[16] has made progress toward numerical techniques well-suited for the analysis of the flow around VAWTs. These numerical tools aid in developing a better physical understanding of the VAWT wake dynamics, which ultimately leads to more efficient wind farm designs.

Despite the existence of a variety of aerodynamic models and increasing simulation efforts for individual VAWTs, there is a rather limited literature on the performance of arrays of VAWTs. Rajagopalan *et al.*[17] examined the performance of clusters of co-rotating VAWTs by idealizing the rotors as momentum sources in a two-dimensional incompressible flow field. They concluded that the physical positioning of the VAWTs relative to each other had a significant effect on their aerodynamic performance, and that downwind turbine performance within an array could be improved by judicious selection of the turbine positions to maximize the overall array performance. Another VAWT array study was conducted by Whittlesey *et al.*,[18] who showed by a semi-empirical analysis based on potential flow theory that an order-of-magnitude improvement in footprint power density was possible for wind farms comprised of counter-rotating VAWT pairs. This was subsequently supported in full-scale experiments by Dabiri,[10] and additional full-scale experiments have shown that this arrangement of VAWTs allows for a reduction in the average inter-turbine spacing relative to HAWT arrays.[11] What is still lacking, however, is a reliable means to predict the array configurations that would optimize this performance.

It is worth noting that the suggestion of exploiting positive aerodynamic interference effects to boost wind farm performance is not limited to VAWT arrays. Ammara *et al.*[19] adopted a similar approach to that proposed by Rajagopalan *et al.*[17] in their study of HAWTs. Their numerical study revealed that similar positive interference effects can be present in HAWT arrays, such that a strategically designed dense array could produce energy at levels similar to those of a sparse arrangement.

Due to the sensitivity of the overall wind farm efficiency to its layout, identifying the optimal design by experiment alone would be impractical due to the time and expense involved. The practical alternative that most optimization studies for HAWT farms have employed is the use of simplified models either as standalone predictive tools (e.g., Ref. 20) or embedded within higher fidelity numerical simulations (e.g., Ref. 9). The latter work incorporates knowledge

about the complex turbulent flow patterns within a wind farm, which has been shown to be important in the vertical transport of energy.[21] A wind tunnel study by Chamorro and Porté-Agel[22] on the effects of thermal stability and incoming boundary layer flow characteristics on HAWT wakes demonstrated that the velocity deficit at hub height along the center of the wake was a key to the characterization of the overall wake and that its adequate prediction was essential in order to assess performance.

This prior experience in optimizing HAWT array performance motivates our work to develop a simple model to discover and characterize optimal VAWT arrays. We present an application of actuator disk theory for VAWTs within the framework of two-dimensional potential flow theory. Potential flows in general, and source distribution methods in particular, have been used extensively in both naval hydrodynamics (e.g., Refs. 23 and 24) and airplane aerodynamics (see, e.g., the review by Hess[25]) to model inviscid flow past bluff bodies. In the latter review, the author points out that the predictions of such methods have been found to agree well with experiments over a large range of flow conditions. In addition, even when the results do not agree quantitatively with experiments, they are frequently useful in predicting the incremental effect of a proposed design change or in ordering various designs in terms of effectiveness, which is arguably the level of fidelity most useful in a wind farm layout optimization study.

The remainder of the paper is organized as follows: Sec. II describes the analytical potential flow model; Sec. III describes the full-scale field measurements used to validate the model; Sec. IV compares the model predictions with field measurements; and finally, Sec. V summarizes and discusses the contributions of this work.

## II. ANALYTICAL MODEL

The flow around an isolated VAWT is approximated by using a two-dimensional potential flow model consisting of a uniform flow, a potential source, and a potential sink. This can be expressed mathematically by the complex velocity, $W(z)$

$$W(z) = V_\infty e^{-i\alpha} + \left[ \frac{m_{so}}{2\pi z} - \frac{m_{si}}{2\pi(z - z_s)} \right],$$

(1)

where $V_\infty$ is the magnitude of the freestream velocity, $\alpha$ is the freestream angle of incidence, and $m_{so}$ and $m_{si}$ are the source and sink strength, respectively. The source denotes the center of the conceptual VAWT, and it is located at the origin; $z_s$ is the downstream position of the sink. The resulting velocity vector at a point in the flow is $\mathbf{V}(z) = \Re(W)\hat{\mathbf{x}} - \Im(W)\hat{\mathbf{y}}$, where $\hat{\mathbf{x}}$ and $\hat{\mathbf{y}}$ are Cartesian unit vectors.

When the source and sink are of equal strength, closed streamlines are formed in the shape of what is known as a Rankine body. In the present work, we define a "leaky Rankine body" (LRB) that is analogous to the Rankine body, but with a sink that is stronger than the source. The relative strengths of the source and sink are determined by the VAWT power coefficient as described below. A representative comparison between the streamlines around a Rankine body and an LRB with the same source strength and downstream spacing from source to sink (but different sink strength) is shown in Figure 1. Note that the Rankine body is shaded as a black ovoid in Figure 1(a) and that an individual VAWT is shaded as a black circle in Figure 1(b) with a diameter equal to the rotor diameter. To model an array of VAWTs, a superposition of individual LRBs is used. Figure 1(c) shows representative streamlines around a pair of VAWTs. The LRB streamlines have a qualitatively similar appearance to the separated wake of a bluff body. This is used presently to model the effect of each VAWT wake on other VAWTs within an array.

The LRB model implicitly assumes that the flow around each VAWT is steady and irrotational everywhere. The assumption of steady flow is reasonable to first order since the turbine output power typically scales cubically with the mean wind speed at hub height.[8] The assumption of irrotational flow is frequently used in high Reynolds number flows with limited
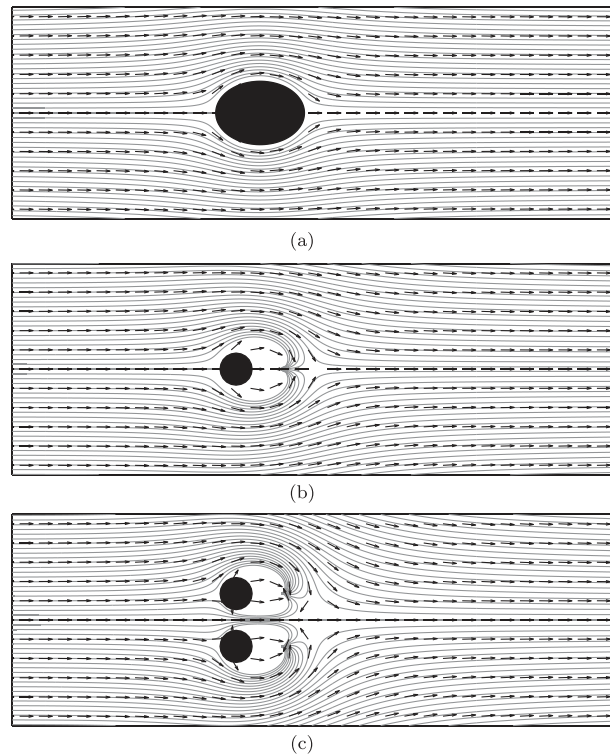
FIG. 1. (a) Streamlines formed by a source and sink of equal strength separated by distance $s_s$. Closed streamlines are shaded with a solid black ovoid, which is known as a Rankine body. (b) LRB streamline pattern formed by a source and sink separated by distance $s_s$. The sink strength in (b) is greater than in (a) with all other parameters the same. The solid black circle indicates the size and position of the VAWT that is modeled. (c) Streamlines formed by the superposition of two LRB models.

separation but is known to lead to an erroneous prediction of zero net drag for any body formed by a closed streamline that encloses all singularities.[26] Hence, if a classical Rankine body were used for the VAWT model, the zero drag prediction would imply that the model turbine does not exchange energy with the flow. However, a branch of potential flow theory known as free-streamline theory has been successfully employed to estimate the drag and shape of the steady wake in cavity flows[27] and behind bluff bodies.[28] More recently, another potential flow model known as the Föppl point vortex system has been used to study vortex dynamics and control for solid bodies.[29,30] An underlying assumption of both the Föppl system and free-streamline theory is that a non-zero drag on a body in potential flow requires that a wake region be modeled explicitly; this is a feature of the LRB model. More precisely, it can be shown that there exists a finite force required to hold a source or a sink in place within a uniform flow.[31] Since the LRB model produces a net sink flow within a uniform flow, the force required to hold these singularities in place is an analogous representation of the drag on the turbine. Thus, the model is similar in physical principle to the actuator disk concept.

    The LRB model for an isolated VAWT is fully specified by three parameters: the source strength $m_{so}$, sink strength $m_{si}$, and downstream spacing from source to sink $s_s$. The source and sink strength are determined by application of Bernoulli's equation and the conservation of mass and momentum (i.e., actuator disk theory) to specify the speed of the flow upstream of each turbine (i.e., $U_2$) and in its far wake (i.e., $U_4$). Given the freestream speed $U_1$, it can be shown that $U_2 = U_1(1 - a)$ and $U_4 = U_1(1 - 2a)$, where the induction factor $a \equiv (U_1 - U_2)/U_1$ is determined from the turbine power coefficient $C_p = 4a(1 - a)^2$. Thus, the primary input to the model is the nominal individual VAWT efficiency. For a given freestream speed $U_1$, and induction factor $a$, the LRB model parameters are related by the following linear system of equations:

$$-aU_1 = -\frac{m_{so}}{2\pi r_u} + \frac{m_{si}}{2\pi(r_u + s_s)}$$
$$-2aU_1 = \frac{m_{so}}{2\pi r_w} - \frac{m_{si}}{2\pi(r_w - s_s)}, \tag{2}$$

where $r_u$ and $r_w$ are the nominal positions of the upstream and far wake flow speeds, respectively. The sink spacing $s_s$, however, remains as a free parameter in this model and is calibrated presently by a least-squares fit to velocity data collected in the field. In the results that follow, the VAWT efficiency is taken as nominally 10%, which is consistent with the field data. The upstream position is set at 3 D in front of each turbine and the far wake is 10 D downstream. It is shown later that the model is relatively insensitive to different quantitative choices for all of the aforementioned input parameters. To be sure, the model does begin to exhibit discrepancies with the field data if the upstream point is less than approximately 3 D away from the turbine, due to the effect of the singularity (i.e., the source) located at the turbine axis.

In the present work, individual VAWTs are located on a Cartesian grid with 0.15 D resolution in the x-y plane. The turbine spacing mimics the configuration of VAWTs described in Sec. III. Because the power produced by each turbine is proportional to the cube of the upstream wind speed, the performance of each array is quantified by the average value of $U_2^3$ over all of the turbines in the array. A more detailed development of the LRB model and its connection to actuator disk theory is given in the Appendix.

## III. EXPERIMENTAL METHODS

### A. Field site and wind turbines

Field measurements of an array of full-scale VAWTs (Windspire Energy, Inc.) were conducted in the Antelope valley of northern Los Angeles County in California, USA from 2011 to 2013. The layout of the facility is shown in the photograph in Figure 2. The VAWT array was initially comprised of nine counter-rotating turbine pairs arranged on an equidistant grid spaced 8 D apart with the turbines in each pair separated center-to-center by 1.65 D. Six additional turbines were added subsequently, of which one was used in a study described below. The VAWTs have a lift-based rotor design consisting of three airfoil blades and a rated power output of 1.2 kW. The total height of each turbine is 9.1 m with a rotor height of 6.1 m and a diameter of 1.2 m. The nominal cut-in and cut-out speeds of the turbines are 4 m s$^{-1}$ and 12 m s$^{-1}$, respectively. The turbines operate at a rotation rate of approximately 350 rpm and a tip speed ratio of 2.3 in incident winds of 8 m s$^{-1}$.
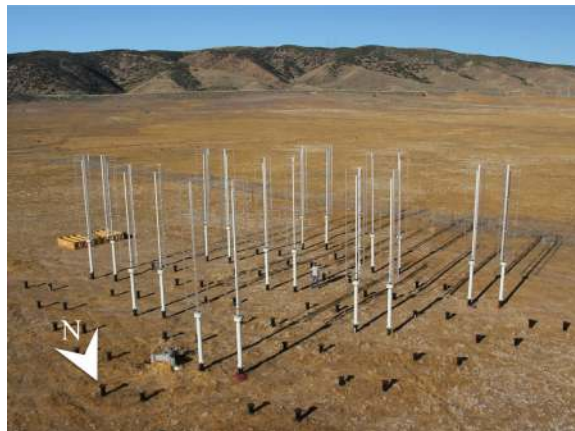


FIG. 2. Photograph of the experimental VAWT array.

## B. Wind velocity measurements

Wind velocity was measured using seven three-component ultrasonic anemometers (Campbell Scientific CSAT3) mounted on a 10 m meteorological tower (Aluma-Towers, Inc.) and vertically spaced in 1 m increments over the turbine rotor height. The CSAT3 sensors were operated at a sampling frequency of 10 Hz with a measurement uncertainty of 0.161 m s$^{-1}$. Both the sensors and the data logger (Campbell Scientific CR3000) were powered by a solar panel and battery system to make the apparatus fully portable. An additional reference meteorological tower was positioned southeast of the array. This 10 m tower continuously recorded both wind speed and direction at 10-min intervals using a cup anemometer (Thies First Class). The data were subsequently uploaded to a database via satellite link.

Vertical profiles of wind velocity were measured at nine positions along the centerline of a four-turbine array as indicated in Figure 3(a). The four turbines were aligned with a southwesterly wind direction and the measurement duration at each position was approximately 150 h. Data were also collected with all 18 turbines erected. During this period, vertical profiles of wind velocity were measured at four positions along the centerline of the array as shown in Figure 3(b). For both measurement periods, the prevailing wind direction was from the southwest. For each meteorological tower position, the data were first conditioned to include only wind directions between 215° and 235°. The measured streamwise velocity was then normalized by the reference tower streamwise velocity and averaged spatially over the seven sensors and in time. This resulted in one normalized streamwise velocity measurement, $U$, per measurement location. For comparison with the LRB model, this normalized velocity $U$ at the array centerline position $A_{CL}/D = -15$ in Figure 3(b) was used as the normalized freestream velocity, i.e., $U_\infty$.

## C. Power measurements

Turbine output power was continuously recorded to a Campbell Scientific data logger (CR3000) at 10-min intervals and then uploaded to a database (available at http://flowe.caltech.edu) via satellite link. The power data was conditioned to examine the performance among individual turbines within the 4-turbine array and also the 18-turbine array. The average performance between five 12-turbine subsets of the 18-turbine array was also examined as described below. For each 10-min power measurement, the power coefficient, $C_p = P/\frac{1}{2}\rho A V_\infty^3$, was calculated for each turbine. Here, $P$ is the power produced by the turbine, $\rho = 1.2$ kg m$^{-3}$ is the density of
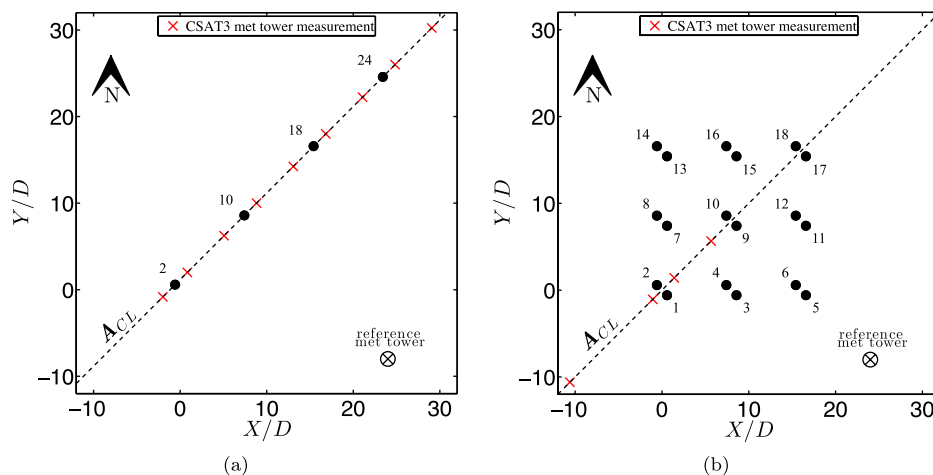


FIG. 3. (a) Schematic top view of the four VAWT array and (b) schematic top view of the 18 VAWT array. VAWTs are drawn to scale with black circles and numbered individually. Velocity measurement positions are indicated by red X's. The position of the reference meteorological tower is not drawn to scale. The axis dimensions are given in rotor diameters where $D = 1.2$ m.

air, $A = 7.3$ m$^2$ is the projected area of the rotor, and $V_\infty$ is the reference meteorological tower wind speed.

Figure 4(a) shows a box plot of the power coefficient for each of the four turbines when all four turbines were simultaneously operational. In this case, power data was only included for wind speeds between 6 and 10 m s$^{-1}$, but all wind directions were allowed in order to examine its effect on performance. A radial histogram of wind direction for this case is shown in Figure 4(c), which also indicates the number of hours of power data collected. The effect of wind direction on turbine performance was obtained by comparing the mean $C_p$ of each turbine for wind directions between 185°–210°, 210°–235°, 235°–260°, 260°–285°, and 285°–310°. A paired student's *t*-test was used to evaluate the statistical significance of each comparison. The result was considered statistically significant if the null hypothesis, i.e., that the difference between the two mean values of $C_p$ was due to random variation, could be rejected with greater than 95% confidence. For the case of the 18-turbine array, the power coefficient for each turbine when all turbines were simultaneously operational is shown in Figure 4(b). In this case,
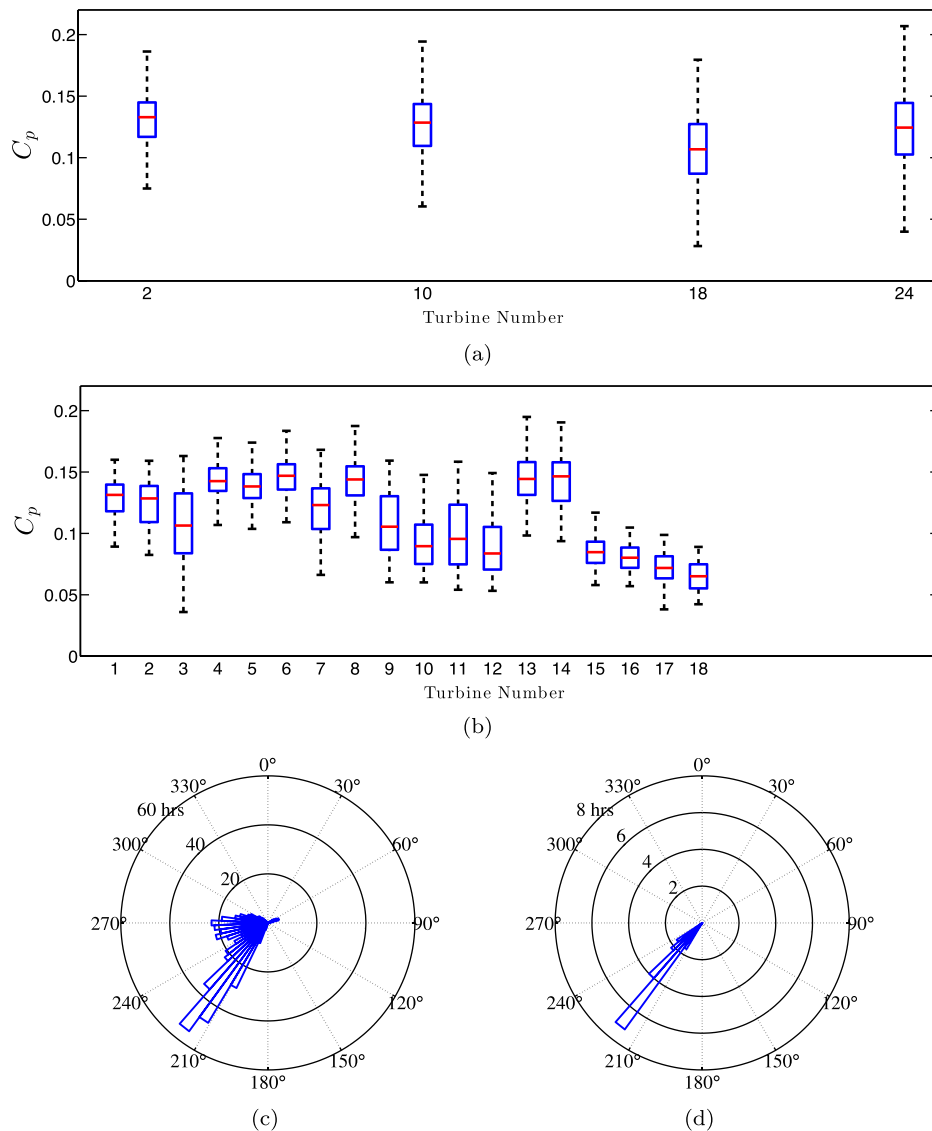


FIG. 4. Box plot of individual turbine power coefficient (a) when four turbines are operational for all wind directions and (b) when 18 turbines are operational and wind direction is between 215° and 235°. (c) Wind rose in degrees from due north for the four-turbine array and (d) the 18-turbine array. Wind speeds are between 6 and 10 m s$^{-1}$ for both cases.

power data was only included for wind speeds between 6 and 10 m s$^{-1}$ and wind direction between 215° and 235°. The corresponding radial histogram is shown in Figure 4(d). Individual turbine performance was examined by calculating an average $C_p$ for each turbine and performing a paired $t$-test between that turbine and each of the other seventeen turbines.

Because not all 18 turbines were continuously operational during the measurement campaign (e.g., due to turbine maintenance), the field measurements also characterized various configurations comprised of subsets of the 18 turbines. We identified five unique array configurations with 12 VAWTs producing power during similar wind conditions (i.e., wind speeds between 6 and 10 m s$^{-1}$ and wind direction between 215° and 235°). These five unique array configurations, shown schematically in Figure 5, were selected for detailed analysis of relative array performance. It was observed that turbines 1 and 2 at the front of the array had a different $C_p$ for each of the different configurations. This was attributable to differences in wind conditions during the measurement of each configuration, rather than to an inherent difference in efficiency for each configuration. To account for this, the $C_p$ of each turbine in each array was normalized by the average $C_p$ of the front two turbines in that array. The relative performance of the arrays, i.e., the average of the normalized $C_p$ for each configuration, was compared using a paired $t$-test.

## D. LRB model calibration

The centerline meteorological tower data for a single VAWT and a VAWT pair were both used to determine the sink spacing, $s_s$, for the LRB model. For the single VAWT (cf. Figure 3(a)), only the measurement locations at $A_{CL}/D = -2$, 2, and 8 were used to give velocity measurements around the first turbine in the array. Velocity measurements at $A_{CL}/D = -15$ were taken only for the VAWT pair but were also used with the single VAWT data. For the VAWT
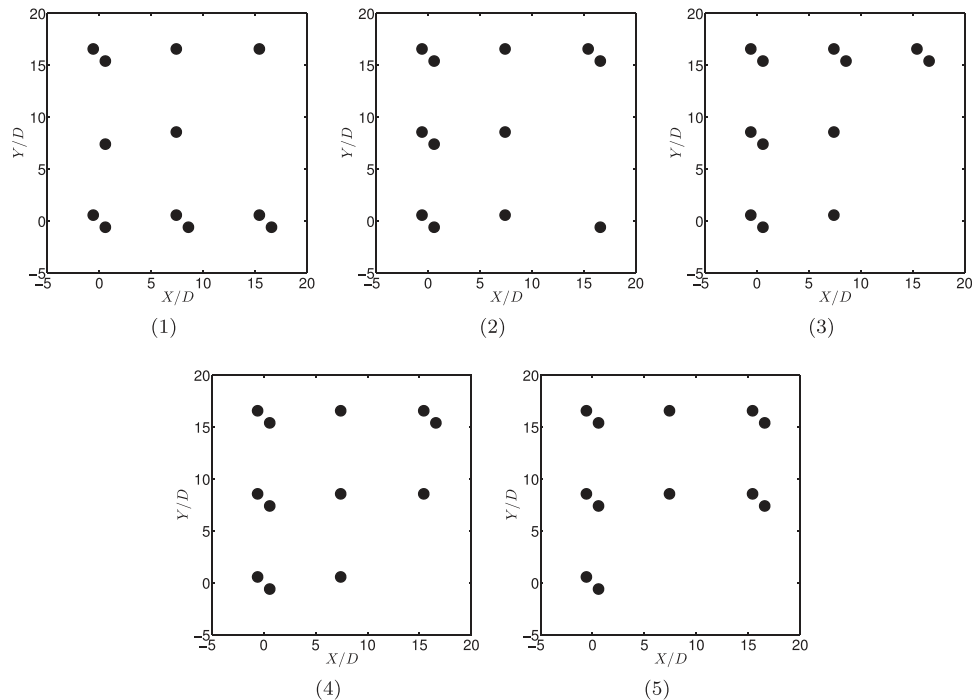


FIG. 5. Five 12-turbine array configurations selected for analysis of relative array performance. The power data for each configuration is a subset of the data collected from the full 18-turbine array when only 12 turbines are producing power with wind speeds between 6 and 10 m s$^{-1}$ and wind direction between 215° and 235°. Only turbines that are operational are indicated by the solid black circles. Configuration (1) includes 43 ten-minute average data points, configuration (2) includes 15 data points, configuration (3) includes 31 data points, configuration (4) includes 47 data points, and configuration (5) includes 12 data points.

pair (c.f. Figure 3(b)), all of the measurement locations were used in the calibration, i.e., $A_{CL}/D = -15, -1.5, 2,$ and 8. The calibration consisted of finding the sink spacing that minimized, in the least-squares sense, the difference in the model prediction of the velocity and the field data at the specified positions.

As shown in Figures 6(a) and 6(b), the best-fit curves to the respective data sets achieve reasonable agreement between the LRB model and the field measurement. However, rather than using two different values for $s_s$ (i.e., one from the single VAWT calibration and one from the VAWT pair), an intermediate value of $s_s/D = 1.44$ is used subsequently for all of the LRB model predictions. This value was obtained by minimizing the sum of the least-squares error between the field data and the respective LRB model predictions. The sensitivity of the LRB model to the choice of $s_s$ is quantified in Sec. IV C. It is worth noting that the point directly behind the single turbine, i.e., $A_{CL}/D = 2$, sits very close to a singularity, i.e., the potential sink, which makes an LRB prediction of velocity at this point very sensitive to small changes in the flow field.

The calibrated LRB model was used to reconstruct the remainder of the centerline meteorological tower velocity data for the four-turbine array as shown in Figure 7. There is reasonable agreement between the model and the field data beyond the original four calibration points. Notably, the best agreement with the LRB model is seen directly in front of the each turbine, which is most important for predicting turbine performance. The worst agreement is directly behind each turbine due to the aforementioned model sensitivity near the singularities.
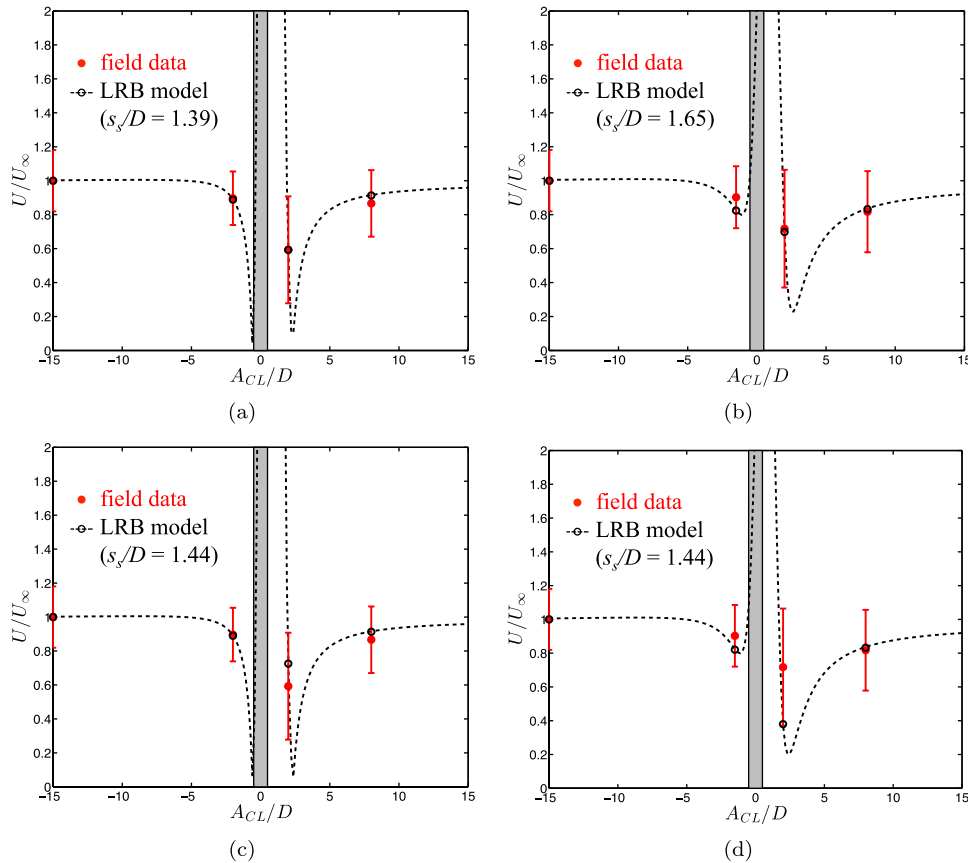


FIG. 6. Calibration of the sink spacing model parameter, $s_s$. (a) Least-squares fit to the field data for the single VAWT. (b) Least-squares fit to the field data for the VAWT pair. Best fit model parameter, $s_s/D = 1.44$, to the combined field data for the (c) single VAWT and (d) pair of VAWTs. Open black circles indicate the LRB model prediction of flow speed at the field measurement locations. Gray rectangles indicate turbine positions.
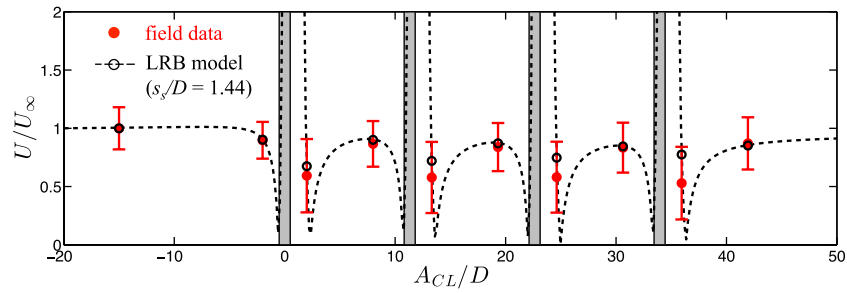
FIG. 7. Comparison of the LRB model with meteorological tower streamwise velocity measurements for the four-turbine array. Open black circles indicate the LRB model prediction of flow speed at the field measurement locations. Gray rectangles indicate turbine positions.

## IV. RESULTS

### A. LRB model prediction of individual turbine performance

Figure 8 shows the effect of wind direction variation on turbine performance for the four-turbine array. Figure 8(a) indicates the bins for wind direction that were used to sort the field
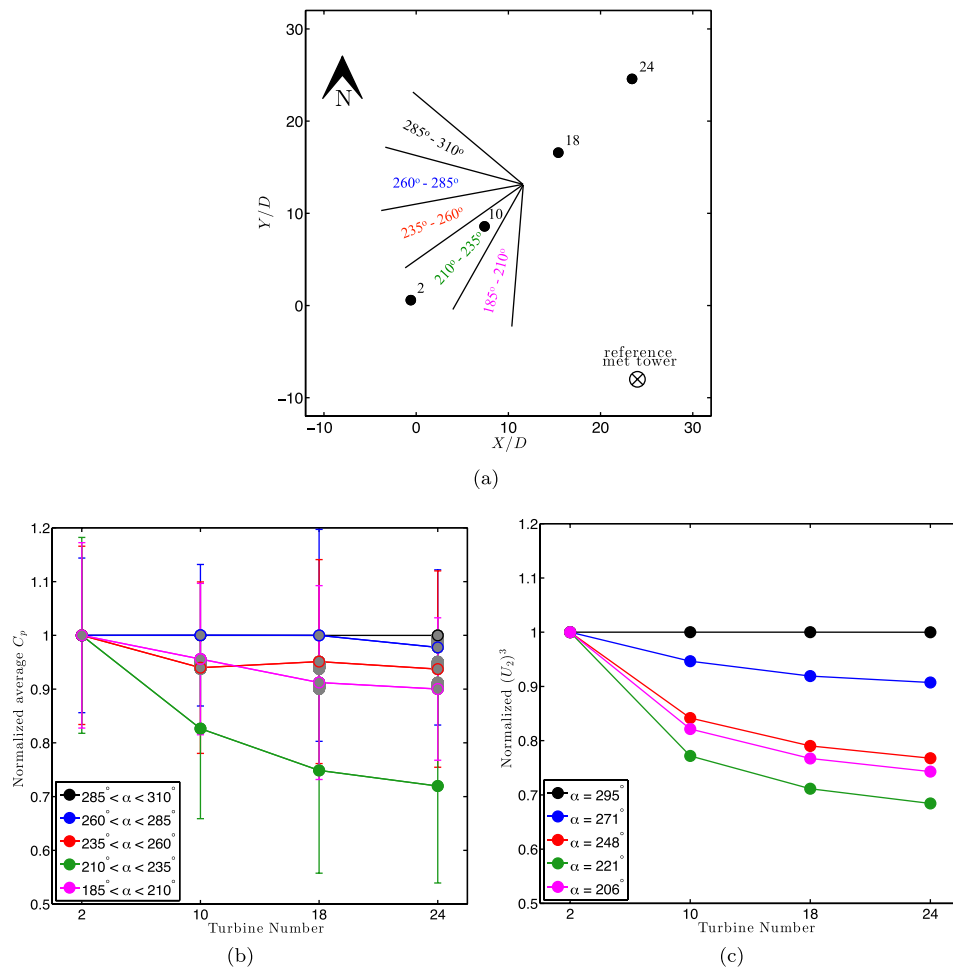


FIG. 8. The effect of wind direction on turbine performance for the indicated four-turbine array. (a) Schematic of the array with the bins of wind direction. (b) Field measurements of individual turbine performance. Error bars indicate one standard deviation. (c) LRB model prediction of turbine performance for each wind direction, taken as the average in each bin.

data. The variation of the individual turbine $C_p$ with wind direction is shown in Figure 8(b). The LRB model prediction of individual turbine performance is shown in Figure 8(c).

For each data point in Figure 8(b), the mean $C_p$ for a given turbine and wind direction has been normalized as follows: The mean $C_p$ of each turbine was first normalized by its mean $C_p$ when the wind was near perpendicular to the array (i.e., 285°–310°). An exception is for turbine 18, which had erroneous velocity data when the wind velocity was between 285° and 310°. Hence, the $C_p$ for turbine 18 was normalized by the average $C_p$ when the wind direction was between 260° and 285°. The normalized $C_p$ was then divided by the $C_p$ of the lead turbine (i.e., turbine 2) to give the relative trend among the turbines.

The result of each *t*-test between pairs of data points in Figure 8(b) is shown graphically using closed symbols to denote mean values that are statistically significantly different when compared to any other data point, and open symbols to denote mean values that are not statistically significantly different between points that coincide within the gray region. For example, for turbine 10, the blue data point is directly on top of the black data point, and is indicated by an open blue symbol filled with gray. This blue point is greater than the red, pink, and green data point; similarly, the solid green data point is lower than all of the rest. However, the difference between the red and pink data points is not statistically significant, as indicated by open symbols connected by a gray bar.

The LRB model results shown in Figure 8(c) are normalized in an analogous manner as the field data. There is reasonable agreement between the field measurements and the LRB model, which is able to capture the qualitative trends in individual turbine performance and also correctly predicts the ordering of the colored curves. The best turbine performance occurs when the wind is nearly perpendicular to the array (black curve) and the worst turbine performance occurs when the wind is nearly parallel to the array (green curve), as would be expected intuitively. What is less intuitive is the slope of these curves, i.e., the percent change in performance of one turbine downstream of another. It can be seen that there is good agreement again between the LRB model and the field data for the limiting case of incident wind nearly parallel to the array. However, the LRB model tends to over predict the effect of the wake as the wind direction moves around toward perpendicular to the array. The field data indicates that when the wind direction is greater than approximately 270°, there is no loss in performance due to the wake of the upstream turbines. However, for a wind direction of 271° (i.e., the mean of the 260°–285° bin), the LRB model predicts a monotonic decrease in performance for each turbine, ending with a loss of power of about 10% at turbine 24 relative to turbine 2. Similarly, the LRB model amplifies the magnitude of the power lost among the downstream turbines for the intermediate wind directions, which indicates that the modeled LRB wake is broader than the actual VAWT wake. This overprediction of power loss suggests that the LRB model, while effective in capturing the rank ordering of turbine performance, is a conservative estimate of array performance.

Figure 9 shows a comparison between the field data and the LRB model for the 18-turbine array configuration when all turbines are simultaneously operational. The average wind direction of 222° is used for the LRB model prediction. The mean $C_p$ for a given turbine is normalized by the average $C_p$ of the front two turbines, i.e., turbines 1 and 2. Qualitatively, there is good agreement between the plots of the field data and that of the LRB model. During the measurement campaign, turbines 3 and 7 experienced a number of maintenance issues. This is reflected in the large variance in turbine 3 and the relatively low performance of both turbines.

While it is possible that other discrepancies between the two plots in Figure 9 are due to individual variations among the turbines, we are not able to quantify these effects because the individual performance characteristics of each turbine in isolation are unknown. However, if we assume that each turbine in the array is identical, as they ideally should be, then the qualitative agreement with the LRB model gives some insight into the characteristics of the flow within the array. One interesting feature is that both the field data and the LRB model indicate that there are specific turbines within the array that perform better than the front two turbines. Specifically, the LRB model predicts that turbines 3, 4, 6, 7, 8, and 13 all perform better than the front two turbines to some degree. Similarly, the field data shows that turbines 4, 5, 6, 8, 13, and 14 consistently perform better than the
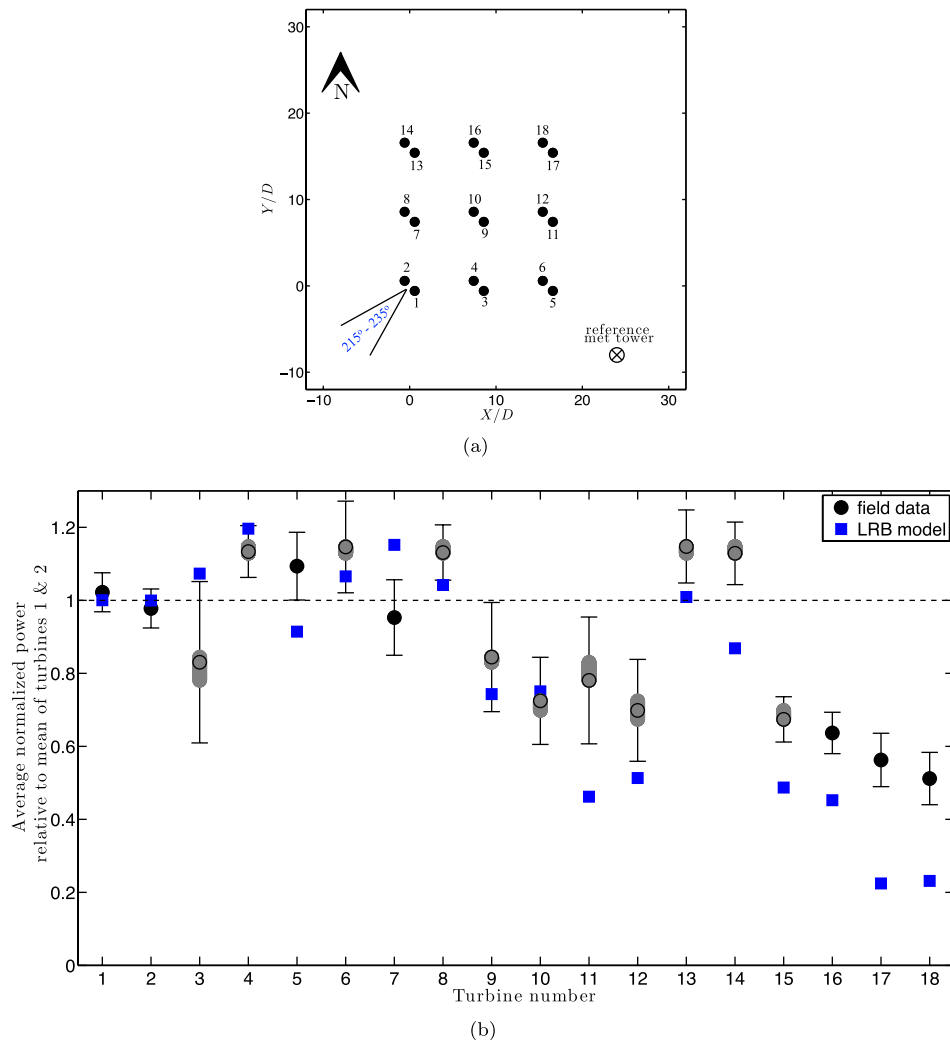
FIG. 9. (a) Schematic of the 18-turbine array with the bin of wind direction. (b) Comparison of field measurements and LRB model prediction for the performance of individual turbines within the array. Error bars indicate one standard deviation.

front two turbines. This seems to suggest that a position such as that of turbine 4, which is slightly set back within the array, has an inherent aerodynamic advantage over, e.g., turbine 1, 2, or 3. The physical mechanism that promotes such an advantage is addressed in Sec. IV B. Also of interest is that the LRB model seems to under predict the performance of turbines 5 and 14, which are on the outer corners of the array. This discrepancy is attributed to the overly broad nature of the LRB wake as previously observed.

## B. LRB model prediction of turbine array performance

While it is desirable to accurately predict the percent change in power loss for individual turbines within an array, a primary goal of the proposed low-order model is to be able to predict differences in average performance between unique array configurations. As discussed in Sec. III, a subset of five unique turbine configurations from the 18-turbine array was examined for this purpose. Figure 10 shows a comparison between the field measurements and the LRB model prediction of array performance for the five unique turbine configurations.

The most significant result is that the LRB model correctly predicts the ranking of all of the array configurations to within statistical certainty. Specifically, the performance of both
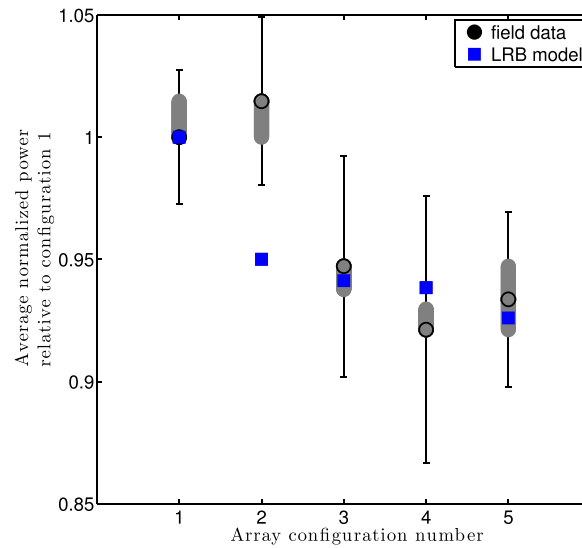
FIG. 10. Comparison of field measurements and LRB model prediction of average array performance for the five unique configurations of twelve VAWTs. Error bars indicate one standard deviation.

configurations 1 and 2 are found to be greater than 3, 4, and 5 with greater than 95% confidence that the null hypothesis can be rejected. There is a seemingly large discrepancy between the LRB model prediction and the field data for array configuration 2. One possible explanation for this is the aforementioned tendency for the model to overpredict the wake effect. Configuration 1 has nine turbines on the front edges of the array facing into the freestream whereas configuration 2 only has eight (cf. Figure 5). Therefore, it is reasonable to expect that configuration 1 performs better than configuration 2, as the LRB model suggests. However, the limited sample size of each of the subset turbine configurations is such that the difference in performance between configurations 1 and 2 was not found to be statistically significant (as indicated by the vertical gray bars). While the difference in performance between configurations 3 and 5 and also 4 and 5 is not statistically significant, the difference in performance between configurations 3 and 4 is significant. In each case where the measured difference in array performance is statistically significant, the LRB model prediction of array performance is in agreement with this result. It is noteworthy that the magnitude of the difference in performance
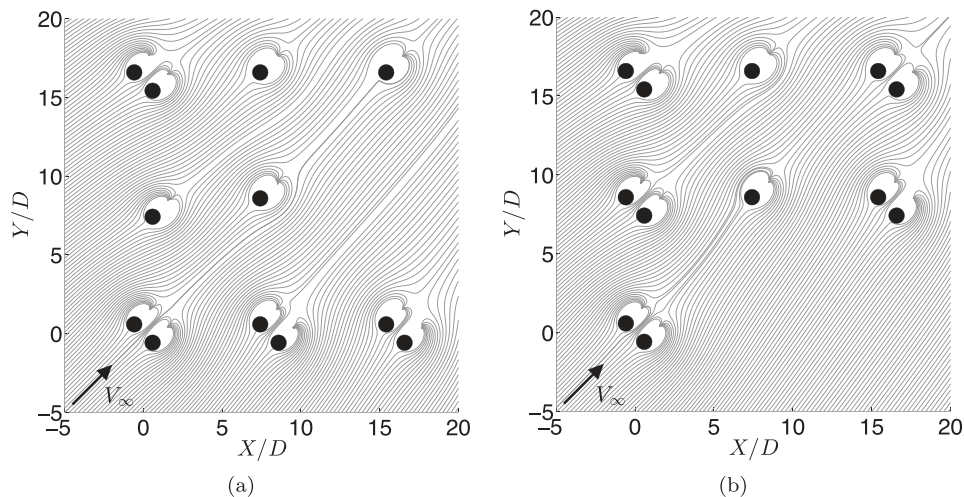


FIG. 11. Streamlines generated by the LRB model for the (a) best and (b) worst performing arrays as predicted by the model, i.e., configurations 1 and 5, respectively.

among the arrays in this case is modest, not exceeding about 10%, and even less than 1% between the LRB model predictions. Yet the model is nonetheless effective in correctly identifying the relative array performances.

Using the LRB model, we can now identify the physical mechanisms that lead to enhanced array performance. A qualitative comparison between the streamlines of the best and worst array configuration is shown in Figures 11(a) and 11(b), respectively. An immediate observation is that the best array configuration has the greatest number of turbines exposed to the freestream. However, this metric is insufficient to distinguish between all five configurations. For example, configurations 3 and 4 have the same number of turbines exposed to the freestream, yet configuration 3 exhibits better performance than configuration 4. For further investigation, smaller two- and three-turbine array configurations can be examined.

Figure 12(a) shows a schematic of a two-turbine array configuration in which turbine A is moved diagonally in front of turbine B. The total array performance, i.e., the average of $U_2^3$ of the two turbines, as a function of the position of turbine A is shown in Figure 12(c). The average value of $U_2^3$ has been normalized by the value for an isolated turbine. As expected, the curve is symmetric about the point where the two turbines are aligned with the freestream. There is also a region that is approximately 4 D wide where the wake of the upstream turbine negatively impacts array performance. Interestingly, the best orientation for the two turbines occurs when turbine B is just slightly outside of the wake region of turbine A, where there is
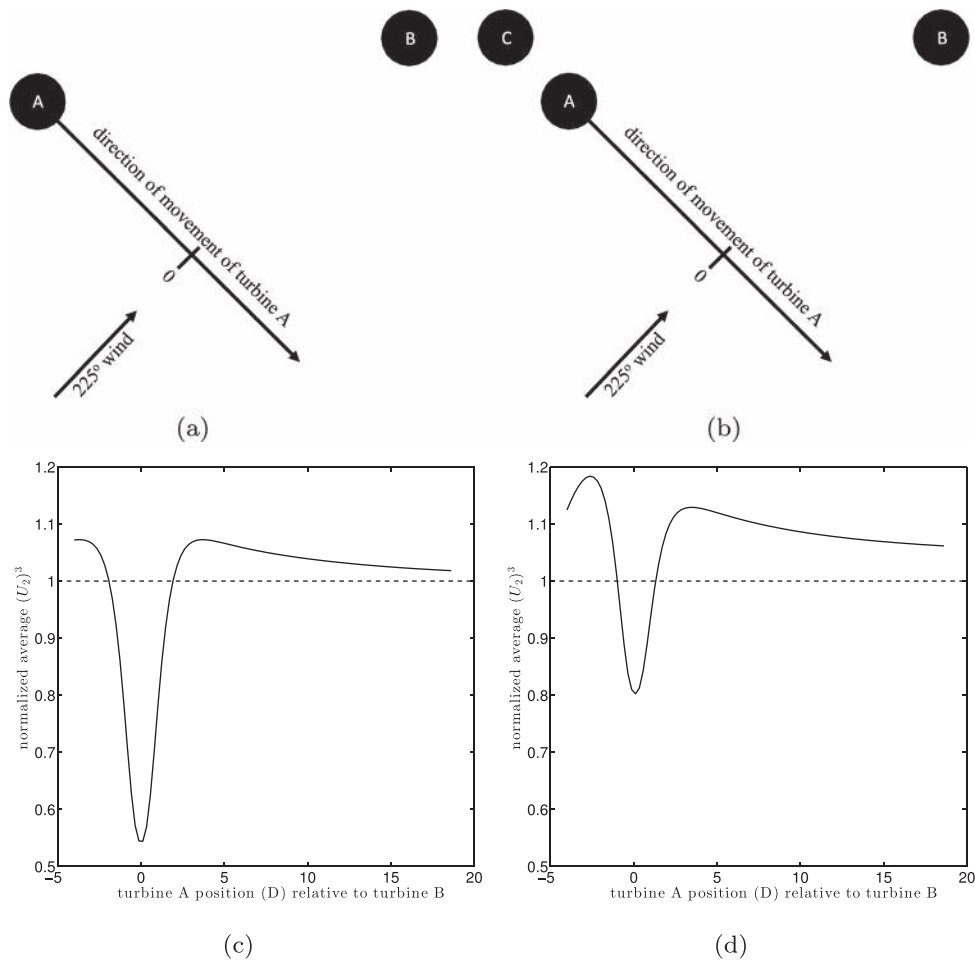


FIG. 12. (a) Schematic for a two-turbine array and (b) three-turbine array, and the LRB model prediction of array performance for each, (c) and (d), respectively. Turbines are drawn to scale with the initial position of turbine A indicated in the figures.

an increase in performance of about 7% relative to the turbines in isolation. A similar result has been observed in previous field experiments.[10] Beyond this point, the normalized array performance asymptotically decreases toward 1 as the turbines are spread further apart.

Figure 12(b) shows a similar schematic as in Figure 12(a), but with an additional turbine that is fixed in place adjacent to turbine A. Again, turbine A is moved diagonally across the line indicated in the plot. The total array performance as a function of the position of turbine A is shown in Figure 12(d). There is now an asymmetry to the array performance curve about the point where turbines A and B are aligned with the freestream due to the presence of the third turbine. The best array performance occurs when turbine A is in between turbines C and B. Furthermore, the entire curve has shifted upward relative to the two-turbine configuration due to the addition of turbine C. There is also a noticeable reduction in the difference between the best and worst configurations, as indicated by the shallower drop in array performance when turbine A is directly in front of turbine B. The LRB model suggests a competition within the array between turbine blockage that can locally accelerate the flow and wake losses that slow the flow down. Optimal array configurations will position turbines to exploit local flow acceleration and avoid regions of wake loss.

## C. Robustness of LRB model prediction of array performance

The robustness of the LRB model depends on its sensitivity to the choices of $C_p$, $r_u$, $r_w$, and $s_s$. In the present evaluation, the LRB model is considered to remain effective if it accurately predicts the ranking of the array configurations in Figure 10. To test the model, the nominal turbine efficiency is varied from 5% to 59% (i.e., the Betz limit); $r_u/D$ is varied from 1 to 6; and $r_w/D$ is varied from 5 to 10. The results for these test cases are shown in Figures 13(a)–13(f). In these figures, the black circles indicate that the LRB model correctly predicts the array ranking and an "X" indicates that the model fails. The red circle indicates the nominal values of the LRB model. This test shows that the model prediction is robust to increases in the value used for $C_p$ but that it fails when $C_p$ is too low (5%) and for very large $C_p$ (59%).

Two cases were considered to evaluate the effect of varying the sink spacing, one with $s_s/D = 1.0$ and another for $s_s/D = 2.0$. Figures 14(a) and 14(b) show that the LRB model is relatively insensitive to these choices of the sink spacing parameter, which are considered extreme cases given the small difference in least-squares estimates of $s_s$ during the model calibration.

## V. CONCLUSIONS

The low-order LRB model has been developed to rapidly distinguish the performance of arbitrary configurations of VAWT arrays. Comparison with field measurements validated that the LRB model is able to not only asses differences among individual turbines within an array but also to predict the ranking of the average performance of unique VAWT arrays with better than 95% statistical certainty. The LRB model is conservative in that it overpredicts the losses caused by the turbine wakes. In conjunction with the field data, the LRB model also provides insight into the physical mechanisms that determine individual turbine dynamics and array performance. A key conclusion that can be drawn from the present results is that there are two primary competing fluid dynamic mechanisms within the array that contribute to the overall performance. The first is turbine blockage, which can locally accelerate the flow adjacent to a turbine and, perhaps surprisingly, can thereby increase the performance of neighboring turbines above their performance in isolation. The other effect is that of the turbine wake, which locally decelerates the flow and leads to a decrease in performance for downstream turbines. The combined effect is captured by the LRB model, and therefore it achieves a reasonable estimate of performance based on the average wind speed directly ahead of each turbine.

It is prudent to note that this simplified model is not intended to capture the complex structure and dynamics of the three-dimensional turbulent flow that occurs in wind farms, e.g., the vertical shear of the incoming atmospheric boundary layer, or the dynamics of the energy exchange between the atmospheric boundary layer and the array. Rather, the model is intended to serve as a tool that can rapidly assess, to a first approximation, the viability of one wind
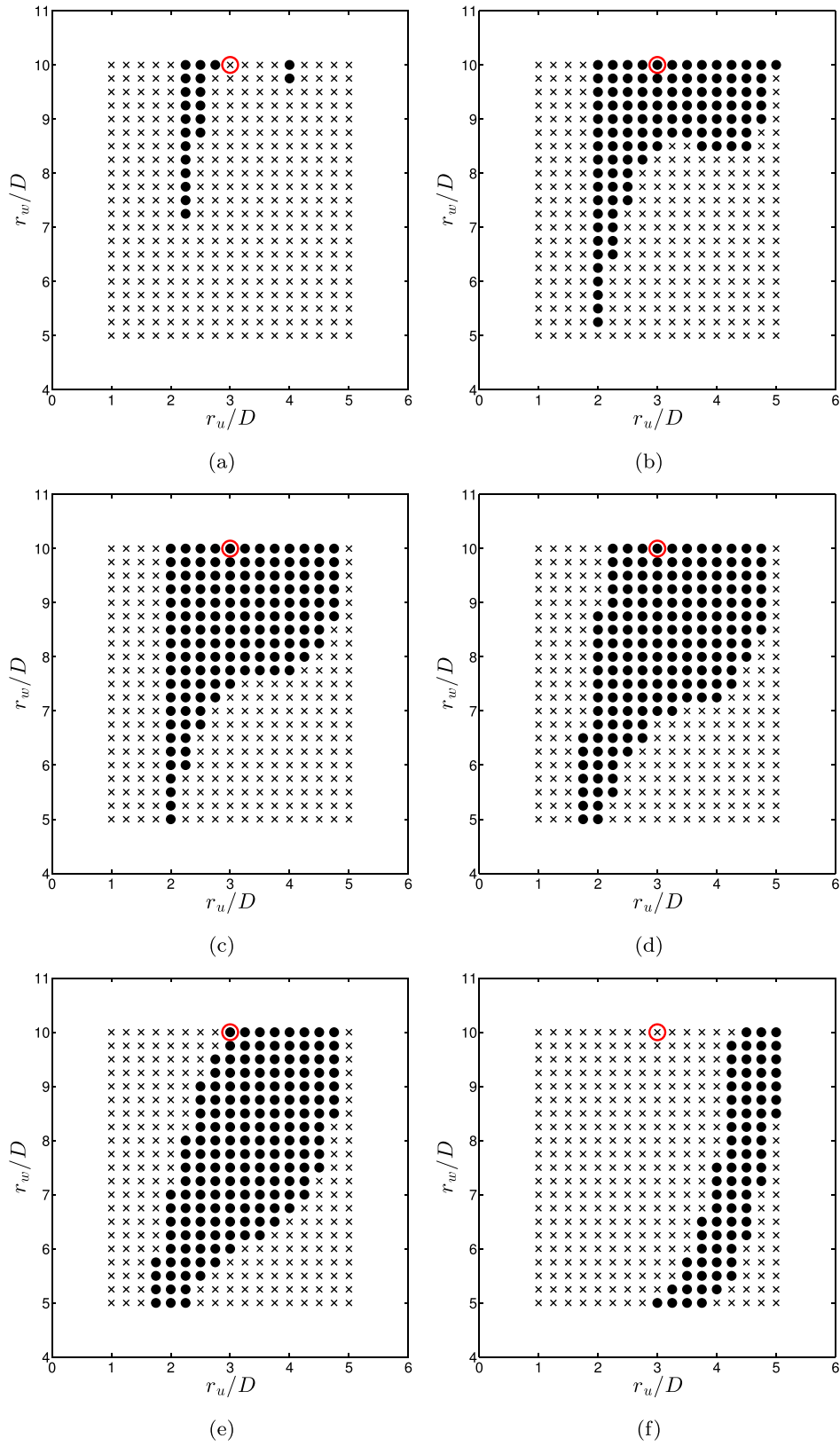
FIG. 13. Parameter study of the LRB model prediction of array performance with varying $C_p$ as (a) 5%, (b) 10%, (c) 15%, (d) 20%, (e) 30%, and (f) 59%. Black circles indicate the model correctly predicts the ordering of array performance and black Xs indicate where the model fails. The red circle indicates the nominal model parameters of $r_u/D = 3$ and $r_w/D = 10$.

FIG. 14. Parameter study of the LRB model prediction of array performance with varying the sink spacing, $s_s$, model parameter. (a) $s_s/D = 1.0$ and (b) $s_s/D = 2.0$. Black circles indicate the model correctly predicts the ordering of array performance and black X's indicate where the model fails. The red circle indicates the nominal model parameters of $r_u/D = 3$ and $r_w/D = 10$.
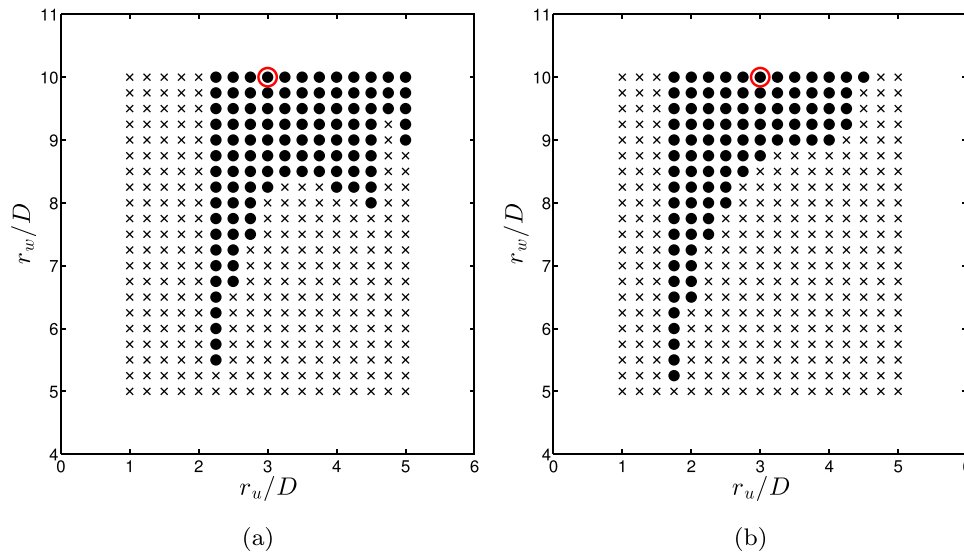
farm configuration relative to another. This approach is akin to the work of Betz, which despite assumptions of inviscid flow among other simplifications, can be quite useful for performing engineering calculations of wind turbines. Additionally, the benefit of the current approach is that optimal array configurations can be found with significantly less computational expense than higher fidelity numerical simulations such as LES and much more rapidly than in experiments. Future work will explore the applicability of the present method for design of HAWT farms.

## ACKNOWLEDGMENTS

## APPENDIX: DETAILED DEVELOPMENT OF THE LRB MODEL

The purpose of this section is to provide additional background information and details on the development of the LRB model. As introduced in Sec. II, the LRB model is an application of the simplified model of wind turbine aerodynamics known as actuator disk theory.[3,8] In what follows, actuator disk theory is briefly reviewed and then related to the LRB model via potential flow theory.

In actuator disk theory, the turbine rotor is idealized as a permeable, non-rotating disk and the flow is assumed to be one-dimensional, frictionless, and incompressible. Mass is conserved and thus the velocity is continuous along a streamtube that encompasses the disk. A key assumption of the theory is the presence of a discontinuous pressure drop across the disk, which is an idealization of the mechanical extraction of energy by the turbine. An example schematic of this flow with the corresponding velocity and pressure distribution is shown in Figure 15. The lines drawn in this figure are only for illustrative purposes as the theory only stipulates the conditions at stations 1–4. Determination of the full distribution of velocity and pressure requires solution of the equations of fluid motion, e.g., by direct numerical simulation. Conservation of mass requires that
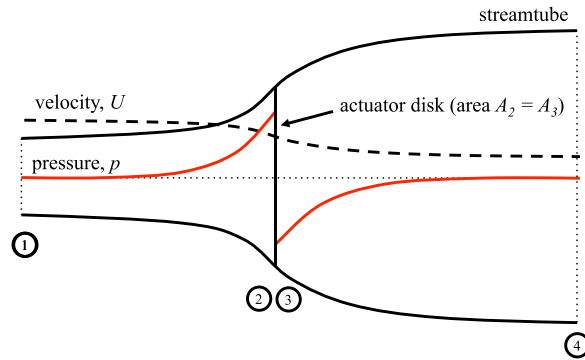
FIG. 15. Schematic of the flow through a turbine modeled as an actuator disk. The variable streamtube cross-sectional area, velocity, and static pressure fore and aft of the turbine are indicated.

$$\dot{m} = \rho U_1 A_1 = \rho U_2 A_2 = \rho U_4 A_4, \tag{A1}$$

where $U_1$, $U_2$, and $U_4$, are the flow velocities upstream of the rotor, at the rotor, and in the far wake of the rotor, respectively. Note from Figure 15 that $U_3 = U_2$ and $A_3 = A_2$, but that $p_3 < p_2$. Another key assumption of the theory is that the static pressure in the far wake (i.e., station 4) fully recovers to the value upstream (i.e., station 1), or $p_4 = p_1$. Applying Bernoulli's equation from station 1 to 2 and again from station 3 to 4 gives the following two equations for the static pressure directly in front of and behind the disk:

$$p_2 = \frac{1}{2}\rho U_1^2 + p_1 - \frac{1}{2}\rho U_2^2, \tag{A2}$$

$$p_3 = \frac{1}{2}\rho U_4^2 + p_4 - \frac{1}{2}\rho U_3^2. \tag{A3}$$

The magnitude of the force, $F$, acting on the disk is then $F = (p_2 - p_3)A_2$. By linear momentum conservation it can be shown that

$$\dot{m}(U_4 - U_1) = (p_2 - p_3)A_2. \tag{A4}$$

Combining Eqs. (A1)–(A4) give the following result for the velocity directly in front of the rotor:

$$U_2 = \frac{1}{2}(U_1 + U_4). \tag{A5}$$

The axial induction factor, $a$, is defined as the following:

$$a \equiv \frac{U_1 - U_2}{U_1}. \tag{A6}$$

By algebraic manipulation of Eqs. (A5) and (A6), it can be shown that

$$U_2 = U_1(1 - a), \tag{A7}$$

$$U_4 = U_1(1 - 2a). \tag{A8}$$

Finally, the power, $P$, extracted from the flow by the turbine is given by $P = FU_2$, which upon substitution of Eqs. (A4) and (A5) gives

$$P = \frac{1}{2}\rho A_2 U_2 (U_1^2 - U_4^2). \tag{A9}$$

The turbine power coefficient, $C_p$, is defined as

$$C_p \equiv \frac{P}{\frac{1}{2}\rho A_2 U_1^3} = 4a(1-a)^2. \tag{A10}$$

It was shown in Sec. II that the LRB model assumes that the mean flow around an individual VAWT can be represented by a potential flow consisting of a uniform flow of magnitude $V_\infty$, a potential source of strength $m_{so}$, and a potential sink of strength $m_{si}$, with the source and sink separated by a distance $s_s$. Without loss of generality, it is illustrative to examine the case of a uniform flow of magnitude $U_1$ in the $x$-direction and with a source and sink placed along the $x$-axis. This results in a streamwise velocity along the $x$-axis, $U(x)$, which is dependent on the strength of the source and sink as well as their spacing. Assuming that the source is located at the origin, this streamwise velocity is given as follows:

$$U(x) = U_1 + \left[ \frac{m_{so}}{2\pi x} - \frac{m_{si}}{2\pi(x - s_s)} \right]. \tag{A11}$$

The connection between this potential flow velocity profile and the aforementioned actuator disk theory is in the specification of $m_{so}$ and $m_{si}$ in Eq. (A11). Given the $C_p$ of a particular turbine, the induction factor, $a$, is immediately known from Eq. (A10). By further specifying the freestream velocity, $U_1$, the velocities $U_2$ and $U_4$ are given by Eqs. (A7) and (A8), respectively. An important distinction of the LRB model is that the velocity is indeterminate in the region very close to the turbine rotor due to the presence of the singularities. Therefore, it is not possible to sample the velocity directly at the turbine rotor. Instead, the velocity as seen by the rotor, i.e., $U_2$, is taken as the potential flow velocity just upstream of the turbine center at the position $x = -r_u$ in the LRB model. Similarly, the far wake velocity, i.e., $U_4$, is positioned downstream of the turbine center at $x = r_w$. This results in the following system of equations:

$$U(-r_u) = U_2 = U_1 - \frac{m_{so}}{2\pi r_u} + \frac{m_{si}}{2\pi(r_u + s_s)}, \tag{A12}$$

$$U(r_w) = U_4 = U_1 + \frac{m_{so}}{2\pi r_w} - \frac{m_{si}}{2\pi(r_w - s_s)}. \tag{A13}$$

Given the sink spacing, $s_s$, which is calibrated as described in Sec. III, the above system of equations can be solved for $m_{so}$ and $m_{si}$ for a single turbine. Taking $s_s/D = 1.44$, $r_u/D = 3$, and $r_w/D = 10$, the corresponding velocity magnitude (i.e., wind speed) along the $x$-axis given by the LRB model for a single VAWT is shown in Figure 16. In this plot, it can be observed that the velocity as seen by the rotor ($U_2$) is in accordance with Eq. (A5) derived from actuator disk theory, i.e., $0.96 \approx \frac{1}{2}(1 + 0.94)$.

The primary utility of the LRB model is in assessing the performance of arrays of turbines. To do this, individual turbines within an array are modeled by a superposition of LRBs. By this approach, the resulting flow around each turbine in the array is different from the isolated LRB,
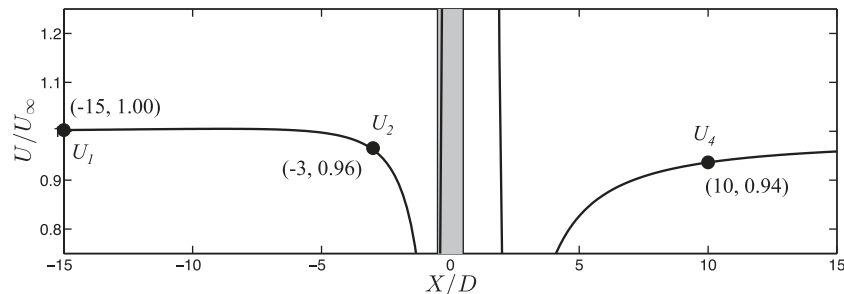


FIG. 16. Axial velocity distribution for a single VAWT by the LRB model. Gray rectangle indicates turbine position.

which implies that the resultant turbine efficiency, i.e., $C_p$, is variable. The benefit of superposition is the speed of calculation (e.g., a few seconds for dozens of VAWTs). The tradeoff, however, is that the actual efficiency of each VAWT in the array is ill-defined because there does not exist an objective freestream (i.e., $U_1$), only the incident speed $U_2$. For a single turbine with a given $C_p$, the turbine power scales as $U_1^3$, i.e., $P \sim U_1^3$. Since $U_1 = U_2/(1-a)$, and $a$ is nominally a constant, then it can be similarly stated that the turbine power scales as the cube of the incident speed, i.e., $P \sim U_2^3$. Hence, this metric is a suitable choice for making relative, as opposed to absolute, predictions of performance among turbine arrays and it is used in the LRB model for just this purpose.

[1]W. J. M. Rankine, "On the mechanical principles of the action of propellers," Trans. Inst. Nav. Archit. **6**, 13 (1865).

[2]D. Yang, C. Meneveau, and L. Shen, "Large-eddy simulation of offshore wind farm," Phys. Fluids **26**, 025101 (2014).

[3]*Wind Turbine Technology: Fundamental Concepts of Wind Turbine Engineering*, edited by D. A. Spera, 2nd ed. (ASME Press, New York, 2009).

[4]M. O. L. Hansen, J. N. Sørensen, S. Voutsinas, N. Sørensen, and H. Aa. Madsen, "State of the art in wind turbine aerodynamics and aeroelasticity," Prog. Aerosp. Sci. **42**, 285 (2006).

[5]A. Betz, "Das maximum der theoretisch möglichen ausnützung des windes durch windmotoren," Z. Gesamte Turbinenwesen **26**, 307 (1920).

[6]P. B. S. Lissaman, "Energy effectiveness of arbitrary arrays of wind turbines," J. Energy **3**, 323 (1979).

[7]P. B. S. Lissaman, G. W. Gyatt, and A. D. Zalay, "Numeric modeling sensitivity analysis of the performance of wind turbine arrays," Technical Report No. PNL-4183, Pacific Northwest Laboratory, 1982.

[8]E. Hau, *Wind Turbines*, 2nd ed. (Springer Verlag, Berlin, 2005).

[9]J. Meyers and C. Meneveau, "Optimal turbine spacing in fully developed wind-farm boundary layers," Wind Energy **15**, 305 (2012).

[10]J. O. Dabiri, "Potential order-of-magnitude enhancement of wind farm power density via counter-rotating vertical-axis wind turbine arrays," J. Renewable Sustainable Energy **3**, 043104 (2011).

[11]M. Kinzel, Q. Mulligan, and J. O. Dabiri, "Energy exchange in an array of vertical-axis wind turbines," J. Turbul. **13**, 1 (2012).

[12]K. J. Touryan, J. H. Strickland, and D. E. Berg, "Electric power from vertical-axis wind turbines," J. Propul. Power **3**, 481 (1987).

[13]M. Islam, D. S.-K. Ting, and A. Fartaj, "Aerodynamic models for Darrieus-type straight-bladed vertical axis wind turbines," Renewable Sustainable Energy Rev. **12**, 1087 (2008).

[14]R. J. Templin, "Aerodynamic performance theory for the NRC vertical-axis wind turbine," Technical Report No. LTR-LA-160, National Aeronautical Establishment Laboratory, 1974.

[15]L. Martinelli and A. J. Smits, "High-fidelity computational fluid dynamics (CFD) for the wind/tidal energy industry," in *Proceedings of the HKIE Civil Division International Conference* (2012), pp. 1–10.

[16]S. Shamsoddin and F. Porté-Agel, "Large eddy simulation of vertical axis wind turbine wakes," Energies **7**, 890 (2014).

[17]R. G. Rajagopalan, T. L. Rickerl, and P. C. Klimas, "Aerodynamic interference of vertical axis wind turbines," J. Propul. Power **6**, 645 (1990).

[18]R. W. Whittlesey, S. Liska, and J. O. Dabiri, "Fish schooling as a basis for vertical axis wind turbine farm design," Bioinspiration Biomimetics **5**, 035005 (2010).

[19]I. Ammara, C. Leclerc, and C. Masson, "A viscous three-dimensional differential/actuator-disk method for the aerodynamic analysis of wind farms," J. Sol. Energy **124**, 345 (2002).

[20]G. Marmidis, S. Lazarou, and E. Pyrgioti, "Optimal placement of wind turbines in a wind park using Monte Carlo simulation," Renewable Energy **33**, 1455 (2008).

[21]M. Calaf, C. Meneveau, and J. Meyers, "Large eddy simulation study of fully developed wind-turbine array boundary layers," Phys. Fluids **22**, 015110 (2010).

[22]L. P. Chamorro and F. Porté-Agel, "Effects of thermal stability and incoming boundary-layer flow characteristics on wind-turbine wakes: A wind-tunnel study," Boundary Layer Meteorol. **136**, 515 (2010).

[23]C. W. Dawson, "A practical computer method for solving ship-wave problems," in *Proceedings of Second International Conference on Numerical Ship Hydrodynamics* (1977), pp. 30–38.

[24]B. Zhang, K. Ma, and Z. Ji, "The optimization of the hull form with the minimum wave making resistance based on Rankine source method," J. Hydrodyn. Ser. B **21**, 277 (2009).

[25]J. L. Hess, "Panel methods in computational fluid dynamics," Annu. Rev. Fluid Mech. **22**, 255 (1990).

[26]G. K. Batchelor, *An Introduction to Fluid Dynamics* (Cambridge University Press, New York, 1967).

[27]G. Birkhoff and E. H. Zarantonello, *Jets, Wakes, and Cavities* (Academic Press, Inc., New York, 1957).

[28]T. Y. Wu, "A wake model for free-streamline flow theory. Part 1. Fully and partially developed wake flows and cavity flows past an oblique flat plate," J. Fluid Mech. **13**, 161 (1962).

[29]B. Protas, "Vortex dynamics models in flow control problems," Nonlinearity **21**, R203 (2008).

[30]G. L. Vasconcelos, M. N. Moura, and A. M. J. Schakel, "Vortex motion around a circular cylinder," Phys. Fluids **23**, 123601 (2011).

[31]L. M. Milne-Thomson, *Theoretical Hydrodynamics* (The Macmillan Company, New York, 1960).